Chemical Science

EDGE ARTICLE

View Article Online
View Journal | View Issue

Cite this: *Chem. Sci.*, 2022, **13**, 9525

All publication charges for this article have been paid for by the Royal Society of Chemistry

Activatable photothermal agents with target-initiated large spectral separation for highly effective reduction of side effects†

Jie Sun,‡[a] Ning Cheng,‡[a] Kai Yin,‡[b] Rongchen Wang,[a] Tianli Zhu,[a] Jinzhu Gao,[a] Xuemei Dong,[a] Chengjun Dong,[a] Xianfeng Gu *[b] and Chunchang Zhao *[a]

Received 2nd May 2022
Accepted 5th July 2022

DOI: 10.1039/d2sc02467e

rsc.li/chemical-science

Photothermal agents (PTAs) with minimized side effects are critical for transforming cancer photothermal therapy (PTT) into clinical applications. However, most currently available PTAs lack true selective activation to reduce side effects because of heavy spectral overlap between photothermal agents and their corresponding products. This study reports the construction of activatable PTAs with target-initiated large spectral separation for highly effective reduction of side effects. Such designed probes involve two H_2O_2-activatable PTAs, **aza-BOD-B1** (single activatable site) and **aza-BOD-B2** (multiple activatable site). After interacting with H_2O_2, **aza-BOD-B1** only displays a mild absorption redshift (60 nm) from 750 nm to 810 nm with serious spectral overlap, resulting in a mild photothermal effect on normal tissues upon 808 nm light irradiation. In contrast, **aza-BOD-B2** displays a large absorption spectral separation (150 nm) from 660 nm to 810 nm, achieving true selective activation to minimize side effects during PTT of cancer. Besides, *in vitro* and *in vivo* investigations demonstrated that **aza-BOD-B2** can specifically induce photothermal ablation of cancer cells and tumors while leaving normal sites undamaged, whereas **aza-BOD-B1** exhibits undesirable side effects on normal cells. Our study provides a practical solution to the problem of undesired side effects of phototherapy, an advance in precision medicine.

Introduction

Cancer, as one of the most complicated diseases, threatens human life and health seriously.[1–3] So far, the therapy methods for cancer mainly include surgery, chemotherapy, radiotherapy, *etc.* However, invasive surgical treatment is always accompanied by great physical pain, and radiation therapy or chemotherapy is more likely to be associated with fatal side effects. Therefore, there is a considerable demand to develop more efficient strategies to combat cancer.[4–9] Photothermal therapy (PTT), a new type of tumor treatment, has attracted immense attention because of its non-invasiveness, low toxicity, real-time control, high tumor specificity, and so on.[10–17] PTT treatment utilizes a photothermal reagent to produce heat upon laser irradiation for killing the cancer cells in the exposed area.[18–22] Compared with traditional "always-on" photothermal agents, activatable photothermal agents will suppress cancer precisely and minimize side effects on normal tissue. Although it has been reported that various photothermal reagents can be activated by the tumor microenvironment (hypoxia,[23–25] lower pH,[26–29] overexpression of biological enzymes,[30–32] and reactive oxygen species (ROS)[33–35]),the majority of them have a significant shortcoming: heavy spectral overlap between the photothermal agents and their corresponding products. That is, they are unable to achieve true selective activation and minimize side effects on adjacent normal tissues.

The photothermal agents with a single activatable site cannot change its electronic nature well before and after being activated, and thus the spectral changes are limited. We explored whether it is possible to introduce multiple activation sites into the photothermal agents and then change their structure greatly, causing a large spectral change to achieve truly selective activation. Hydrogen peroxide (H_2O_2) is an important and the most abundant endogenous reactive oxygen species (ROS) in cells.[36,37] Compared with normal cells (the concentration of H_2O_2 below 5 μM), the level of H_2O_2 will be elevated abnormally in cancer cells,[38,39] and thus, it is a good target for designed activatable photothermal agents. Previously, researchers reported a series of activatable photothermal reagents,[40–45] but most of them cannot achieve true selective activation to reduce side effects. So, exploring true selective activatable photothermal reagents with minimal side effects is still quite challenging in this research field. In this contribution, taking H_2O_2 as an example, we proved that the introduction of multiple activation sites on the photothermal

[a]Key Laboratory for Advanced Materials, Feringa Nobel Prize Scientist Joint Research Center, Institute of Fine Chemicals, School of Chemistry and Molecular Engineering, East China University of Science and Technology, Shanghai, 200237, P. R. China. E-mail: zhaocchang@ecust.edu.cn

[b]Department of Medicinal Chemistry, School of Pharmacy, Fudan University, Shanghai, 201203, P. R. China. E-mail: xfgu@fudan.edu.cn

† Electronic supplementary information (ESI) available. See https://doi.org/10.1039/d2sc02467e

‡ These authors contributed equally to this work.

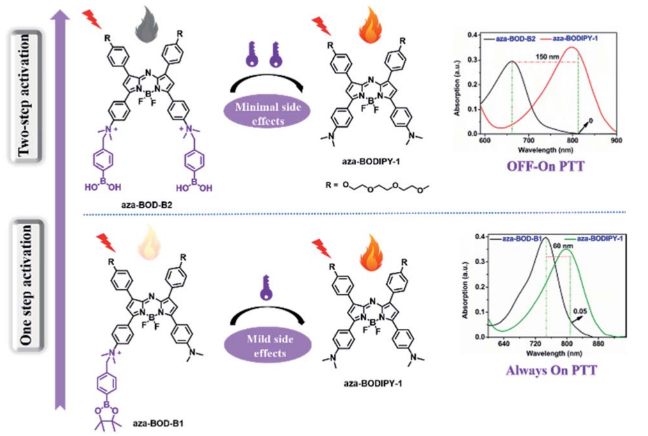

Scheme 1 Rational design of NIR photothermal reagents with H_2O_2-activated large spectral separation for highly effective reduction of side effects during PTT of cancer.

agents is an effective strategy to achieve high efficiency and minimal side effects for photothermal therapy of cancer.

Herein, activatable photothermal agents with target-initiated large spectral separation were reported for highly effective reduction of side effects. Based on the aza-BODIPY backbone (**aza-BODIPY-1**), near-infrared organic photothermal reagents **aza-BOD-B1** (single activatable site) and **aza-BOD-B2** (multi-activatable site) were rationally constructed (Scheme 1). The aza-BODIPY dye was used due to its intense adjustable near-infrared absorption, good optical stability, and large molar extinction coefficient.[46–49] It's worth noting that **aza-BOD-B2** with multi-activatable sites displayed a large absorption redshift (about 150 nm) from 660 nm to 810 nm upon activation by H_2O_2, affording the two well-separated absorption bands that benefit the true selective activation. However, **aza-BOD-B1** with a single activatable site only displayed a mild absorption redshift (about 60 nm) with serious spectral overlap. Correspondingly, under the irradiation of an 808 nm laser, **aza-BOD-B1** exhibits a mild photothermal effect, whereas **aza-BOD-B2** has almost no photothermal effect. In contrast, the H_2O_2-activated product **aza-BODIPY-1** displays excellent photothermal conversion efficiency. Thus, **aza-BOD-B2** can act as a promising candidate for the reduction of side effects efficiently during precise PTT of cancer. *In vitro* investigations have demonstrated that **aza-BOD-B2** is very deadly to H_2O_2-rich cancer cells (A549 cells) and causes minor harm to normal cells (HEK-293T cells), while **aza-BOD-B1** causes significant damage to both types of cell. We further demonstrated that **aza-BOD-B2** can realize precise and efficient treatment for H_2O_2-rich cancer cells and minimize side effects on normal tissue in a mouse model. We envisaged that the multiple-site-activated design strategy for photothermal reagents will facilitate boosting the specificity and precision of cancer photothermal therapy.

Results and discussion

Synthesis of NIR photothermal regents

Based on an NIR-absorbing aza-BODIPY derivative, two near-infrared H_2O_2-activated photothermal regents (**aza-BOD-B1** and **aza-BOD-B2**) were constructed by adjusting the number of the H_2O_2 recognition group. And the introduction of three trimethylene glycol monomethyl ether chains enhanced the water solubility of the two photothermal reagents. The synthesis route is depicted in Scheme S1.† All the chemical structures were identified by ^1H NMR, ^{13}C NMR and HRMS spectrometry.

Spectroscopic properties of aza-BOD-B1 and aza-BOD-B2

First, the spectroscopic properties of **aza-BOD-B1** and **aza-BOD-B2** in response to H_2O_2 were investigated in a buffer solution (PBS/acetonitrile = 1 : 1; pH = 7.4), respectively. As shown in Fig. 1 and S1,† the maximum absorption wavelength (λ_{max}) of **aza-BOD-B1** (single activatable site) is initially at 750 nm, which gradually redshifts to 810 nm upon the addition of H_2O_2 (300 μM), only displaying a slight absorption peak redshift (about 60 nm). In stark contrast, **aza-BOD-B2** (multi-activatable site) exhibits a significant absorption peak redshift (about 150 nm) from 660 nm to 810 nm upon introduction with H_2O_2 (300 μM). Moreover, the two absorption bands of **aza-BOD-B2** were well-separated at 660 nm and 810 nm. Such larger absorption spectrum changes were ascribed to the conversion of **aza-BOD-B2** into **aza-BODIPY-1**, proven by HRMS analysis (Fig. S2†). These results indicate that the construction of photothermal reagents with multi-activatable sites can better change their electronic nature before and after being activated, resulting in larger absorption spectrum changes, which is an effective strategy to solve the problem of spectral overlap. In addition, the two activatable photothermal agents showed good response to H_2O_2 under weak acid conditions (pH = 6.5–7.4, Fig. S3a and S4a†), indicating their potential application in the general weakly acidic environment of tumors. The absorbance intensity changes at 808 nm exhibited a good linear correlation with increasing H_2O_2 concentration (0–30 μM), and the limit of detection (LOD) was calculated to be 1.36 μM which indicates high sensitivity of **aza-BOD-B2** toward H_2O_2 (Fig. S5†). Furthermore, except for H_2O_2 and $ONOO^-$, the other active substances did not cause the obvious absorption spectrum changes of the two compounds (Fig. S3b and S4b†). Importantly, the expression of $ONOO^-$ is minimal and negligible compared to H_2O_2 in live cells,[50] Overall, **aza-BOD-B1** and **aza-BOD-B2** are highly feasible for application in H_2O_2-activated PTT. In particular, **aza-BOD-B2** interaction with H_2O_2 has produced such a large spectral separation, making it a good candidate for precise treatment of H_2O_2-rich cancers.

Photothermal conversion performance of aza-BOD-B1 and aza-BOD-B2

Based on the fact that **aza-BOD-B1** and **aza-BOD-B2** both showed strong NIR absorption at 808 nm activated by H_2O_2, an 808 nm laser was chosen for irradiation. We continue to investigate the photothermal conversion ability of **aza-BOD-B1** and **aza-BOD-B2** in a buffer solution (PBS/acetonitrile = 1 : 1; pH = 7.4). As shown in Fig. 1 and S6,† the temperature changes of **aza-BOD-B1** and **aza-BOD-B2** in the presence or absence of H_2O_2 are compared. Even in the absence of H_2O_2, the temperature of **aza-BOD-B1** reached 47 °C within 10 min upon 808 nm

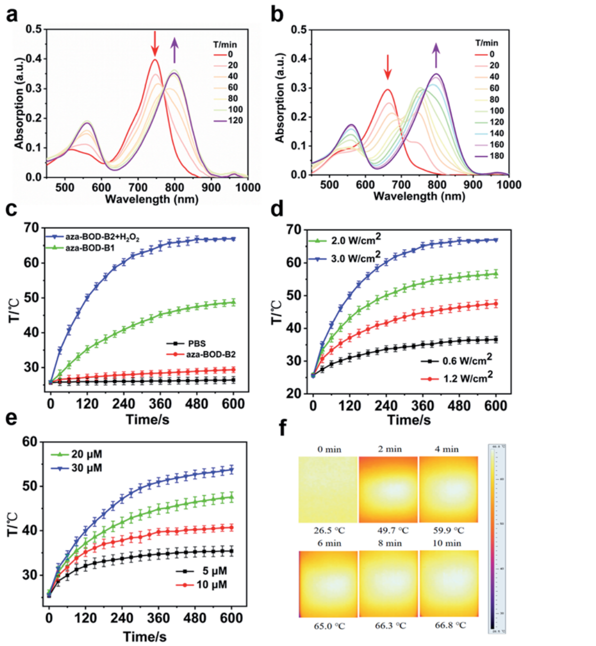

Fig. 1 Time-dependent absorption changes of (a) **aza-BOD-B1** (10 μM) and (b) **aza-BOD-B2** (10 μM) in the presence of 300 μM H_2O_2. (c) Under the 808 nm laser irradiation (3.0 W cm^{-2}), the photothermal temperature curves of PBS, **aza-BOD-B1** (20 μM), **aza-BOD-B2** (20 μM), and **aza-BOD-B2** (20 μM) containing 300 μM H_2O_2. (d) The photothermal temperature change curves of **aza-BOD-B2** (20 μM) activated by H_2O_2 under different power irradiations. (e) Temperature elevation for **aza-BOD-B2** at different concentrations in the presence of H_2O_2 (300 μM) under 808 nm laser irradiation (1.2 W cm^{-2}). (f) Representative IR thermal images of **aza-BOD-B2** (20 μM) in the presence of H_2O_2 (300 μM) under 808 nm laser irradiation (3 W cm^{-2}). Error bars represent the standard error of the mean ($n = 3$).

laser irradiation (3.0 W cm^{-2}). By prominent contrast, the temperature of **aza-BOD-B2** or PBS only exhibited negligible changes under the same conditions (Fig. 1c). The results indicated that **aza-BOD-B1** had a mild photothermal effect even in H_2O_2-deficient noncancerous tissues, whereas **aza-BOD-B2** had almost no such undesired photothermal effect. It should be noted that the temperatures of **aza-BOD-B1** and **aza-BOD-B2** were obviously changed after H_2O_2 activation, indicating that H_2O_2 plays an important role in the transformation of **aza-BOD-B1** or **aza-BOD-B2** into an activatable photothermal agent. Laser power is an important factor that affects the temperature changes of photothermal reagents. As shown in Fig. 1d, the temperature of **aza-BOD-B2** (20 μM) gradually increases as the power density increases, up to 66.8 °C. The temperature change process is recorded with an infrared (IR) thermal image camera (Fig. 1f). Next, we investigated the photothermal effects of different concentrations of **aza-BOD-B2** in the buffer solution. In the presence of H_2O_2, as the concentration (5, 10, 20, and 30 μM) of **aza-BOD-B2** increased, the temperature reached 35 °C, 40 °C, 45 °C, and 53 °C, respectively, upon 808 nm laser irradiation with a power density of 1.2 W cm^{-2}, indicating that it has a good concentration dependence. In addition, time-dependent photothermal temperature changes of **aza-BOD-B1** and **aza-BOD-B2** after H_2O_2 activation under 808 nm laser irradiation (2 W cm^{-2}) showed significant temperature enhancement as the concentration of H_2O_2 increased (Fig. S7†). The photothermal effects of H_2O_2-activated **aza-BOD-B2** were not diminished even after three heating and cooling cycles, indicating good photothermal stability of **aza-BOD-B2** (Fig. S6e†). The H_2O_2-activated photothermal conversion efficiency (η) of **aza-BOD-B2** was determined to be approximately 28.3%. Besides, the two probes exhibited good photostability (Fig. S8†) in buffer solution (PBS/acetonitrile = 1 : 1, pH = 7.4). These favorable results indicate that compared with **aza-BOD-B1**, **aza-BOD-B2** is very promising for H_2O_2-mediated PTT application in living tumors to reduce side effects effectively.

Photothermal cytotoxicity of aza-BOD-B1 and aza-BOD-B2 *in vitro*

Based on the excellent photothermal conversion ability exhibited by **aza-BOD-B1** and **aza-BOD-B2** upon interaction with H_2O_2, their biocompatibility and tumor-specific therapeutic effects were investigated on H_2O_2-rich lung cancer cells (A549) and H_2O_2-deficient human embryonic kidney transformed cells (HEK-293T) using the CCK-8 assay. A549 and HEK-293T cells were treated with **aza-BOD-B1** and **aza-BOD-B2** in different concentrations (0, 5, 10, 20, and 30 μM) for 4 h, respectively. As shown in Fig. 2, the dark toxicity of **aza-BOD-B1** and **aza-BOD-B2** against A549 cells and HEK-293T cells was evaluated. The cellular activity of both cell lines remained higher than 90% even at high concentrations (30 μM) of the two compounds (Fig. 2a and b), indicating that they have good biocompatibility.

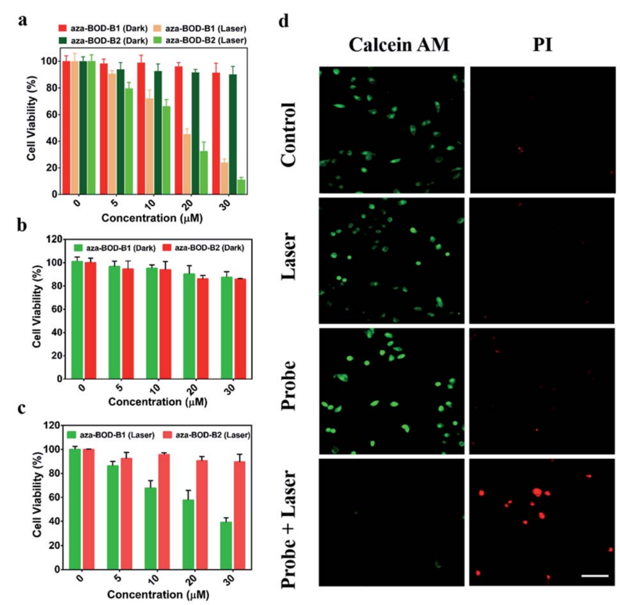

Fig. 2 (a) Viability of A549 cells incubated with **aza-BOD-B1** and **aza-BOD-B2** in the presence or absence of 808 nm laser irradiation. Viability of HEK-293T cells incubated with **aza-BOD-B1** and **aza-BOD-B2** in the absence (b) or presence (c) of 808 nm laser irradiation. (d) Confocal fluorescence images of calcein AM/PI stained A549 cells with different treatments (control, laser only, **aza-BOD-B2** only, and laser + **aza-BOD-B2**). Scale bars: 50 μm. The laser power was 1.2 W cm^{-2}. Error bars represent the standard error of the mean ($n = 5$).

However, considerable cytotoxicity was detected when A549 cells were incubated with **aza-BOD-B1** or **aza-BOD-B2** upon 808 nm laser irradiation. For example, the cell viability was about 40% and 20% after incubation with **aza-BOD-B1** (30 μM) and **aza-BOD-B2** (30 μM) upon 808 nm laser irradiation with a power density of 1.2 W cm^{-2} for 8 minutes of irradiation, indicating the high therapeutic efficacy of **aza-BOD-B1** and **aza-BOD-B2** on cancer cells upon 808 nm light irradiation. What's more, the viability of A549 cells and HEK-293T cells without **aza-BOD-B1** and **aza-BOD-B2** has not been affected under 808 nm laser irradiation (Fig. 2a and c). In addition, **aza-BOD-B2** showed negligible dark cytotoxicity and photocytotoxicity toward normal cells (Fig. 2b and c), suggesting that **aza-BOD-B2** was silent in H_2O_2-deficient cells, which guaranteed minimal side effects on normal tissue. Notably, **aza-BOD-B1** was significantly toxic to normal cells under laser irradiation, the viability of cells being less than 50% at a concentration of 30 μM, implying that **aza-BOD-B1** still exhibits a mild photothermal effect, which resulted in undesirable side effects on normal tissues inevitably. The inhibitory assay with *N*-acetylcysteine (NAC) at the cellular level demonstrated that the activation of these two probes was indeed due to the presence of H_2O_2 (Fig. S9†). These results suggested that **aza-BOD-B2** is a promising tool for H_2O_2-rich cancer photothermal therapy with high precision and minimal side effects.

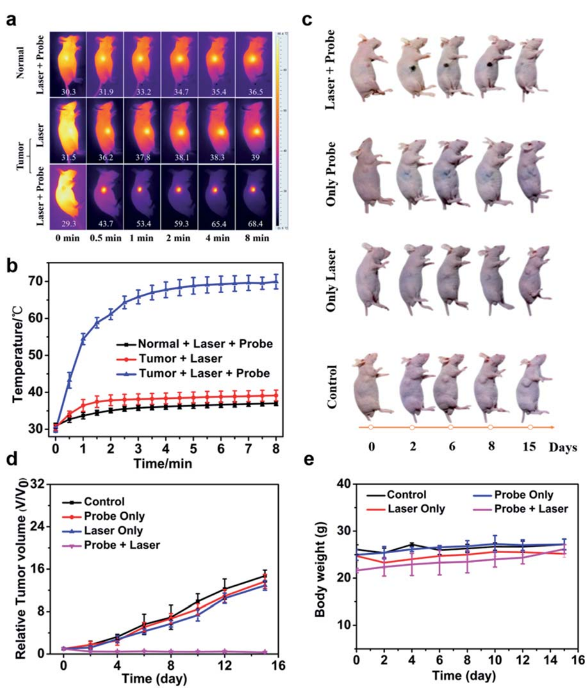

Fig. 3 (a) Infrared thermal images of A549 tumor-bearing mice under continuous NIR laser irradiation with different treatments. Laser irradiation was performed at 4 h post-administration of **aza-BOD-B2**. (b) Mean temperature as a function of irradiation time. Laser irradiation was performed at 4 h post-administration of **aza-BOD-B2**. (c) Representative photos of mice in different groups during the **aza-BOD-B2**-mediated PTT process. (d) Tumor growth curves of mice in different groups by administration of various treatments. (e) Body-weight changes in mice with various treatments. The laser power was 1.2 W cm^{-2}. Error bars represent the standard error of the mean ($n = 5$).

We further performed staining experiments with calcein-AM (live cells, green fluorescence) and PI (dead cells, red fluorescence) to evaluate the effective killing cancer efficacy by **aza-BOD-B2**-mediated photothermal therapy. In the images in Fig. 3d, A549 cells treated with only **aza-BOD-B2** or 808 nm laser irradiation showed no significant cell death. The images of cells that were incubated with **aza-BOD-B2** followed by irradiation with the 808 nm laser (1.2 W cm^{-2}) showed strong red fluorescence and negligible green fluorescence, implying the superior tumor-killing effect of **aza-BOD-B2** under 808 nm laser irradiation.

Photothermal ablation of tumors studies *in vivo*

Inspired by the superior phototherapeutic results of **aza-BOD-B2** on A549 cells *in vitro*, the capacity of **aza-BOD-B2** for photothermal ablation of tumors *in vivo* was then evaluated using A549 tumor-bearing mice; A549 tumor-bearing mice were randomly divided into 4 groups (5 mice in each group) with different treatments (PBS, **aza-BOD-B2**, PBS + laser, and **aza-BOD-B2** + laser). In the laser-irradiated groups, we used an 808 nm laser (1.2 W cm^{-2}) to irradiate the tumor site directly following intratumor 4 h post-injection of PBS or **aza-BOD-B2.** In addition, healthy mice (without tumors) treated with both **aza-BOD-B2** injection and laser irradiation were also investigated to confirm the inactive feature of **aza-BOD-B2** in H_2O_2-deficient normal tissues. Photothermal imaging of tumor regions in A549 tumor-bearing mice injected with **aza-BOD-B2** showed that the tumor temperature rapidly increased to approximately 68.4 °C under the 808 nm laser irradiation for 8 min (Fig. 3a and b). In comparison, there were slight tumor temperature changes in mice treated with only irradiation. Of note, the healthy mice injected with **aza-BOD-B2** also showed a slight increase in temperature (about ∼8 °C) upon 808 nm laser irradiation. These results suggested that **aza-BOD-B2** can only be specifically activated within tumors to achieve effective photothermal conversion, and thus, **aza-BOD-B2** could be a promising tool for efficient therapy of tumors *in vivo*.

To evaluate the *in vivo* treatment effect of **aza-BOD-B2**, the important indexes including mice weight, tumor volume, and the pictures of tumor-bearing mice in different treatment groups at 2, 4, 6, 8, 10, 12, and 15 days after the first administration were recorded. As shown in Fig. 3 and S10,† no obvious therapeutic effect was observed in mice treated with only 808 nm laser irradiation or **aza-BOD-B2**, indicating that **aza-BOD-B2** has negligible dark toxicity. By stark contrast, tumors of mice treated with both **aza-BOD-B2** and laser irradiation were almost completely ablated within 15 days (Fig. 3d), suggesting excellent antitumor efficacy of **aza-BOD-B2.** Notably, no obvious tissue damage was observed when the healthy mice were injected with **aza-BOD-B2** upon laser irradiation (Fig. S10†), which further proved that **aza-BOD-B2** is highly effective in reducing side effects. Mice in each group with various treatments were dissected after 15 days; their tumors and major organs (the heart, liver, spleen, lung, and kidney) were provided for hematoxylin and eosin (H&E) staining analysis to assess the pathological damage caused by **aza-BOD-B2**. The pictures of tumor-bearing mice with different treatments more visually showed that tumor inhibition was significantly enhanced in the **aza-BOD-B2** + laser group compared to the other treatment groups (in Fig. 3c and S10†). Importantly, H&E staining clearly showed significant necrosis in tumors of mice treated with **aza-BOD-B2** and laser irradiation simultaneously, while tumors of mice treated with only **aza-BOD-B2** or 808 nm laser irradiation showed no noticeable histopathological damage (Fig. S11†). In addition, the H&E images of the major organs in various treatment groups indicate minimal histopathological damage. These results indicated that **aza-BOD-B2** has good biocompatibility and safety for *in vivo* application. Lastly, during *in vivo* treatments, a negligible change in mice body weight was observed in all groups (Fig. 3e). These results confirmed that **aza-BOD-B2** is a highly efficient H_2O_2-activated photothermal agent with minimal side effects that can be specifically used for PTT treatment of tumors.

Conclusions

In summary, we developed a photothermal reagent that can achieve true selective activation to reduce side effects for realizing precise PTT therapy of cancer. We have successfully proved that the introduction of multiple activation sites on the photothermal reagent is an effective strategy to significantly eliminate side effects. **aza-BOD-B1** with a single activatable site has a poor spectral separation effect after being activated by H_2O_2 and thus shows a mild photothermal effect under the irradiation of an 808 nm laser in normal tissues, showing undesirable side effects. In sharp contrast, **aza-BOD-B2** can be activated sequentially by H_2O_2 to change its electronic nature well, resulting in two well-separated absorption bands with a large spectral redshift of up to 150 nm. Such significant resolution effectively avoided the problem of spectral overlap and realized true selective activation to reduce side effects upon 808 nm laser irradiation, thus no photothermal effect in normal tissues. In addition, upon activation by H_2O_2, **aza-BOD-B2** exhibited excellent photothermal conversion efficiency under the irradiation of an 808 nm laser, enabling precise PTT treatment in tumor tissues with minimal side effects in normal tissues. *In vivo* tumor inhibition experiments showed that **aza-BOD-B2** could remarkably ablate H_2O_2-rich tumor tissues after 15 days of treatment with minimal side effects. Our study solved the problems of poor specificity and large side effects of traditional photothermal reagents, opening up a new way for precision medicine and the application of photothermal reagents in clinical practice.

Data availability

All the data supporting this paper could be found in ESI.†

Author contributions

J. Sun and N. Cheng performed the synthesis experiments. N. Cheng, R. Wang, T. Zhu and J. Gao collected the optical data and analyzed the experimental data. J. Sun, X. Dong and C. Dong carried out the cell experiments. J. Sun and K. Yin investigated the tumor inhibition experiments. X. Gu and C. Zhao supervised the work and edited the manuscript.

Conflicts of interest

There are no conflicts to declare.

Acknowledgements

We gratefully acknowledge the financial support by the National Natural Science Foundation of China (21874043, 22077030, and 21977018) and the Shanghai Municipal Science and Technology Major Project (Grant No. 2018SHZDZX03).

Notes and references

1 Y. Wang, S. Xu, L. Shi, C. Teh, G. Qi and B. Liu, *Angew. Chem., Int. Ed.*, 2021, **60**, 14945–14953.
2 P. Pei, T. Liu, W. Shen, Z. Liu and K. Yang, *Mater. Horiz.*, 2021, **8**, 1348–1366.
3 R. Wang, K. Yin, M. Ma, T. Zhu, J. Gao, J. Sun, X. Dong, C. Dong, X. Gu, H. Tian and C. Zhao, *CCS Chem.*, 2022, DOI: 10.31635/ccschem.022.202201971.
4 S. Goel, D. Ni and W. Cai, *ACS Nano*, 2017, **11**, 5233–5237.
5 P. Zhu, Y. Chen and J. Shi, *ACS Nano*, 2018, **12**, 3780–3795.
6 P. Huang, X. Qian, Y. Chen, L. Yu, H. Lin, L. Wang, Y. Zhu and J. Shi, *J. Am. Chem. Soc.*, 2017, **139**, 1275–1284.
7 V. Deepagan, D. You, W. Um, H. Ko, S. Kwon, K. Choi, G. Yi, J. Lee, D. Lee, K. Kim, I. Kwon and J. Park, *Nano Lett.*, 2016, **16**, 6257–6264.
8 T. Gu, T. Chen, L. Cheng, X. Li, G. Han and Z. Liu, *Nano Res.*, 2020, **13**, 2209–2215.
9 R. Wang, K. Dong, G. Xu, B. Shi, T. Zhu, P. Shi, Z. Guo, W. Zhu and C. Zhao, *Chem. Sci.*, 2019, **10**, 2785.
10 X. Li, J. Lovell, J. Yoon and X. Chen, *Nat. Rev. Clin. Oncol.*, 2020, **17**, 657–674.
11 H. Sun, Q. Zhang, J. Li, S. Peng, X. Wang and R. Cai, *Nano Today*, 2021, **37**, 101073.
12 D. Li, X. Chen, D. Wang, H. Wu, H. Wen, L. Wang, D. Wang, J. Ji and B. Tang, *Biomaterials*, 2022, **283**, 121476.
13 Y. Zou, W. Liu, W. Sun, J. Du, J. Fan and X. Peng, *Adv. Funct. Mater.*, 2022, 2111853.
14 A. Schwartz-Duval, C. Konopka, P. Moitra, A. Daza, I. Srivastava, E. Johnson, T. Kampert, S. Fayn, A. Haran, L. Dobrucki and D. Pan, *Nat. Commun.*, 2020, **11**, 4530.
15 K. Wang, Y. Xiang, W. Pan, H. Wang, N. Li and B. Tang, *Chem. Sci.*, 2020, **11**, 8055.
16 S. He, Y. Jiang, J. Li and K. Pu, *Angew. Chem., Int. Ed.*, 2020, **59**, 10633–10638.
17 Y. Wang, G. Xia, M. Tan, M. Wang, Y. Li and H. Wang, *Adv. Funct. Mater.*, 2022, 2113098.
18 L. Cheng, X. Wang, F. Gong, T. Liu and Z. Liu, *Adv. Mater.*, 2020, **32**, 1902333.

19 S. Gao, G. Wei, S. Zhang, B. Zheng, J. Xu, G. Chen, M. Li, S. Song, W. Fu, Z. Xiao and W. Lu, *Nat. Commun.*, 2019, **10**, 2206.
20 J. Zhou, L. Rao, G. Yu, T. R. Cook, X. Chen and F. Huang, *Chem. Soc. Rev.*, 2021, **50**, 2839–2891.
21 X. Zhao, S. Long, M. Li, J. Cao, Y. Li, L. Guo, W. Sun, J. Du, J. Fan and X. Peng, *J. Am. Chem. Soc.*, 2020, **142**, 1510–1517.
22 Y. Xu, S. Wang, Z. Chen, R. Hu, Y. Zhao, K. Wang, J. Qu and L. Liu, *Biomaterials*, 2021, **276**, 121017.
23 D. Zhang, Z. Cai, N. Liao, S. Lan, M. Wu, H. Sun, Z. Wei, J. Li and X. Liu, *Chem. Sci.*, 2018, **9**, 7390–7399.
24 H. Wang, K. Xue, Y. Yang, H. Hu, J. Xu and X. Zhang, *J. Am. Chem. Soc.*, 2022, **144**, 2360–2367.
25 T. Zhang, X. Hou, Y. Kong, F. Yang, Y. Yue, M. Shah, H. Li, F. Huang, J. Liu and D. Guo, *Theranostics*, 2022, **12**, 396–440.
26 Y. Li, J. Lin, P. Wang, Q. Luo, H. Lin, Y. Zhang, Z. Hou, J. Liu and X. Liu, *ACS Nano*, 2019, **13**, 12912–12928.
27 B. Yang, Z. Dai, G. Zhang, Z. Hu, X. Yao, S. Wang, Q. Liu and X. Zheng, *Adv. Healthcare Mater.*, 2020, **9**, 1901634.
28 J. Yang, Y. Chen, Y. Li and X. Yin, *ACS Appl. Mater. Interfaces*, 2017, **9**, 22278–22288.
29 Y. Du, D. Wang, S. Wang, W. Li and J. Suo, *RSC Adv.*, 2021, **11**, 6472–6476.
30 J. Li, C. Xie, J. Huang, Y. Jiang, Q. Miao and K. Pu, *Angew. Chem., Int. Ed.*, 2018, **57**, 3995–3998.
31 X. Zhen, J. Zhang, J. Huang, C. Xie, Q. Miao and K. Pu, *Angew. Chem., Int. Ed.*, 2018, **57**, 7804–7808.
32 J. Zhang, P. Cheng and K. Pu, *Bioconjugate Chem.*, 2019, **30**, 2089–2101.
33 Y. Liu, F. Mo, J. Hu, Q. Jiang, X. Wang, Z. Zou, X. Z. Zhang, D. Pang and X. Liu, *Chem. Sci.*, 2021, **12**, 10097–10105.
34 Z. Wang, Z. Xu, P. Upputuri, Y. Jiang, J. Lau, M. Pramanik, Z. Wang, X. Paul, K. Pu and B. Xing, *ACS Nano*, 2019, **13**, 5816–5825.
35 L. Feng, R. Zhao, B. Liu, F. He, S. Gai, Y. Chen and P. Yang, *ACS Appl. Mater. Interfaces*, 2020, **12**, 41047–41061.
36 E. Miller, A. Albers, A. Pralle, E. Isacoff and C. Chang, *J. Am. Chem. Soc.*, 2005, **127**, 16652.
37 B. Dickinson and C. Chang, *J. Am. Chem. Soc.*, 2008, **130**, 9638.
38 T. Szatkowski and C. Nathan, *Cancer Res.*, 1991, **51**, 794–798.
39 H. Zhu, J. Li, X. Qi, P. Chen and K. Pu, *Nano Lett.*, 2018, **18**, 586–594.
40 Y. Li, J. Lin, P. Wang, Q. Luo, H. Lin, Y. Zhang, Z. Hou, J. Liu and X. Liu, *ACS Nano*, 2019, **13**, 12912–12928.
41 H. Wang, Q. Chen and S. Zhou, *Chem. Soc. Rev.*, 2018, **47**, 4198–4232.
42 B. Shi, Q. Yan, J. Tang, K. Xin, J. Zhang, Y. Zhu, G. Xu, R. Wang, J. Chen, W. Gao, T. Zhu, J. Shi, C. Fan, C. Zhao and H. Tian, *Nano Lett.*, 2018, **18**, 6411–6416.
43 B. Shi, N. Ren, L. Gu, G. Xu, R. Wang, T. Zhu, Y. Zhu, C. Fan, C. Zhao and H. Tian, *Angew. Chem., Int. Ed. Engl.*, 2019, **58**, 16826–16830.
44 G. Xu, W. Guo, X. Gu, Z. Wang, R. Wang, T. Zhu, H. Tian and C. Zhao, *CCS Chem.*, 2020, **2**, 527–538.
45 X. Zhao, K. Zhao, L. Chen, Y. Liu, J. Liu and X. Yan, *Chem. Sci.*, 2021, **12**, 442.
46 M. Li, Y. Xu, M. Zhao, F. Li, W. Feng, T. Feng, S. Liu and Q. Zhao, *Inorg. Chem.*, 2020, **59**, 17826–17833.
47 Y. Xu, S. Wang, Z. Chen, R. Hu, S. Li, Y. Zhao, L. Liu and J. Qu, *J. Nanobiotechnol.*, 2021, **19**, 37.
48 Z. Shi, X. Han, W. Hu, H. Bai, B. Peng, L. Ji, Q. Fan, L. Li and W. Huang, *Chem. Soc. Rev.*, 2020, **49**, 7533–7567.
49 Y. Liu, N. Song, L. Chen, S. Liu and Z. Xie, *Chem.–Asian J.*, 2018, **13**, 989–995.
50 S. Parvez, M. J. C. Long, J. R. Poganik and Y. Aye, *Chem. Rev.*, 2018, **118**, 8798–8888.